Available online at www.sciencedirect.com
ScienceDirect
International Journal of Impact Engineering 35 (2008) 885–894
INTERNATIONAL JOURNAL OF IMPACT ENGINEERING
www.elsevier.com/locate/ijimpeng

Static and low-velocity impact behavior of sandwich beams with closed-cell aluminum-foam core in three-point bending

Jilin Yu*, Erheng Wang, Jianrong Li, Zhijun Zheng

CAS Key Laboratory of Mechanical Behavior and Design of Materials, University of Science and Technology of China, Hefei, Anhui 230026, PR China

Received 16 May 2007; received in revised form 21 January 2008; accepted 23 January 2008
Available online 8 February 2008

Abstract

In this paper, the response and failure of sandwich beams with aluminum-foam core are investigated. Quasi-static and low-velocity impact bending tests are carried out for sandwich beams with aluminum-foam core. The deformation and failure behavior is explored. It is found that the failure mode and the load history predicted by a modified Gibson's model agree well with the quasi-static experimental data. The failure modes and crash processes of beams under impact loading are similar to those under quasi-static loading, but the force-displacement history is very different. Hence the quasi-static model can also predict the initial dynamic failure modes of sandwich beams when the impact velocity is lower than 5 m/s.

Keywords: Sandwich beam; Aluminum foam; Low-velocity impact; Failure map; Dynamic response

1. Introduction

Sandwich beams are widely used in many engineering fields due to their advantages over the conventional structural constructions such as high bending stiffness and good weight saving [1]. The behavior of sandwich beams depends on the properties of core material, especially under impact loading [2]. It is important to choose high-quality core material in the optimal design of sandwich beams. As a new multi-function engineering material, aluminum foams have many useful properties such as low density, high stiffness, good impact resistance, high energy absorption capacity, easy to manufacture into complex shape, good erosion resistance, etc. [3,4]. This fact opens a wide range of potential applications for sandwich beams with aluminum-foam core.

Sandwich beams fail by a number of competing mechanisms under both static and impact loading, depending on the geometry of the beam and the relative strength of the face sheets and core [5,6]. Ashby et al. [6] and McCormack et al. [7] established a sandwich beam failure model (named as Gibson's model in this paper), and estimated the initial failure load and the peak failure load based on the deformation forms in different failure modes, i.e. face yielding, face wrinkling, core yielding and indentation. Some parallel research works confirm this model [8,9].

The dynamic behaviors of sandwich structures, especially low-velocity impact behavior, have been widely investigated. Many of these works are experimental studies on the behavior of honeycomb and polymer foam core sandwich structures. Abrate [2] summarized five main dynamic failure modes of such structures with composite face sheets, namely core yield, debonding, core crack, beam crack and fiber crack in face sheet. Fatt and Park [10] defined different dynamic failure modes of polymer foam core and composite face sheet sandwich panels: top face sheet failure, core shear failure and bottom face sheet failure. Xu and Rosakis [11] and Crupi et al. [12] also documented a series of complex failure modes. Dynamic models, such as mass-spring model [2,10] and energy balance model [13], were used to predict the peak load and the load history of sandwich structures. Finite element codes were used to simulate the deformation process [14–17].

*Corresponding author. Tel.: +86 551 360 0792; fax: +86 551 360 6459.
E-mail address: jlyu@ustc.edu.cn (J.L. Yu).

0734-743X/$ - see front matter © 2008 Elsevier Ltd. All rights reserved.
doi:10.1016/j.ijimpeng.2008.01.006

However, only limited data are available for the low-velocity impact behavior of metal foam core sandwich structures. Yu et al. [18] studied the impact behavior and failure mechanism of aluminum face sheet/open-cell aluminum-foam core sandwich beams. It was found that the crush load under impact loading is larger than that under quasi-static loading but the energy absorption is reduced. Since the face sheet and core thickness investigated in [18] is in a narrow range, they found that the beams fail mainly by a face yield mode. Villanueva and Cantwell [19] showed that the glass fiber-reinforced composite face sheet/ALPORAS aluminum-foam core sandwich beams were capable of absorbing large amounts of energy through crushing of the core material and permanent fracture of the top skin. Recently, Xu et al. [20] studied the low-velocity transverse impact behavior of square aluminum alloy tubes filled with aluminum foam. The perforation behavior [21] and the blast loading behavior [22] were also investigated.

In this paper, Gibson's model is modified to accommodate unsymmetric deformation and cylindrical loading head and supports. A failure mode map is constructed for three failure modes. The responses of sandwich beams with aluminum alloy skins and closed-cell aluminum-foam core under quasi-static and low-velocity impact bending are then investigated experimentally and the deformation and failure mechanisms are compared with theoretical predictions.

2. Theoretical analysis

2.1. Elastic deformation of sandwich beams

Consider a sandwich beam of span L and width b loaded in three-point bending (Fig. 1). The thicknesses of the face sheets and core are t and c, respectively. Young's modulus and yield strength of the face material are E_f and σ_{yf}, and Young's modulus, shear modulus, compressive strength and shear strength of the core material are E_c, G_c, σ_{yc} and τ_{yc}, respectively. The deflection of the sandwich beam under load P is given by [7]

$$\delta = \frac{PL^3}{48(\mathrm{EI})_{\mathrm{eq}}} + \frac{PL}{4(\mathrm{AG})_{\mathrm{eq}}}, \tag{1}$$

where $(\mathrm{EI})_{\mathrm{eq}}$ is the equivalent flexural rigidity and $(\mathrm{AG})_{\mathrm{eq}}$ the equivalent shear rigidity defined as

$$(\mathrm{EI})_{\mathrm{eq}} = \frac{E_f bt^3}{6} + \frac{E_c bc^3}{12} + \frac{E_f bt(t+c)^2}{2} \approx \frac{E_f btc^2}{2}, \tag{2a}$$

$$(\mathrm{AG})_{\mathrm{eq}} = \frac{b(c+t)^2 G_c}{c} \approx bcG_c. \tag{2b}$$

2.2. Modified Gibson's model

Instead of a flat loading head and supports used in the experiments and analysis in [7], a cylindrical loading head and supports are used in the present experiments and analysis. Hence some modifications are required. Three main failure modes of metallic foam-core sandwich beams, i.e. face yielding, core shearing and indentation, are considered here, as defined in [7].

The critical load for the face yield mode is given by

$$P_{\mathrm{cri\,fy}} = \frac{4bt(c+t)}{L}\sigma_{\mathrm{yf}}, \tag{3}$$

where the core strength is ignored [7].

Two symmetrical core shear modes were assumed in Gibson's model [7]. The critical loads of core shear mode A with plastic hinges at the loading point and mode B with plastic hinges at the loading point and the supports are

$$P_{\mathrm{cri\,csA}} = \frac{2bt^2}{L}\sigma_{\mathrm{yf}} + 2bc\left(1 + \frac{2H}{L}\right)\tau_{\mathrm{yc}} \tag{4a}$$

and

$$P_{\mathrm{cri\,csB}} = \frac{4bt^2}{L}\sigma_{\mathrm{yf}} + 2bc\tau_{\mathrm{yc}}, \tag{4b}$$

respectively, where H is the overhang length. However, our experiments show that an unsymmetrical deformation mode with plastic hinges only at one support may also occur, as shown in Fig. 2. A similar phenomenon was also observed in Ref. [12].

In fact, when a shear crack occurs in one side of the sandwich beam, the shear stress in the other side will be released. So, the core shear failure may not occur in that side. The modified critical load is then

$$P_{\mathrm{cri\,cs}} = \frac{3bt^2}{L}\sigma_{\mathrm{yf}} + 2bc\left(1 + \frac{H}{L}\right)\tau_{\mathrm{yc}}. \tag{5}$$

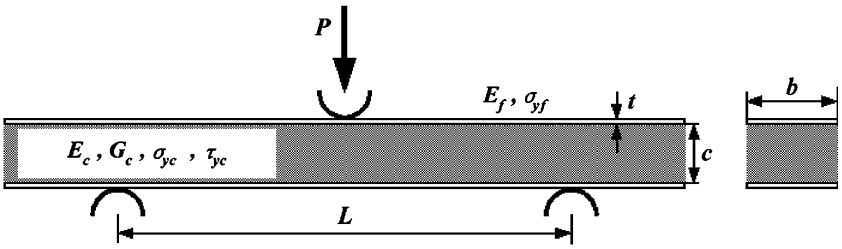

Fig. 1. A sketch of sandwich beam loaded in three-point bending.

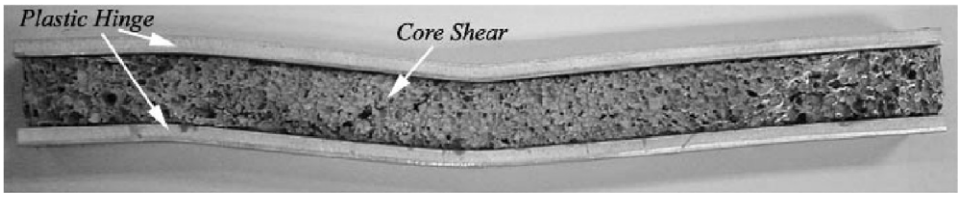

Fig. 2. Core shear failure mode observed in experiments.

The critical load of the indentation mode, $P_{\text{cri in}}$, in Ref. [7] was given as

$$P_{\text{cri in}} = 2bt\sqrt{\sigma_{\text{yf}}\sigma_{\text{yc}}} + ab\sigma_{\text{yc}}, \tag{6}$$

where a is the width of the loading head.

When a cylindrical loading head and supports are used, Eq. (6) should be replaced by [9]

$$P_{\text{cri in}} = 2bt\sqrt{\sigma_{\text{yf}}\sigma_{\text{yc}}}. \tag{7}$$

2.3. The failure mode map

Taking dimensionless parameters t/L and c/L as coordinates, we can construct a failure mode map of sandwich beams under three-point bending from Eqs. (3), (5) and (7). The map is divided into three fields, within which one failure mechanism is dominant. The equations of the transition lines are

$$\frac{c}{L} = \frac{1}{2}\left(\frac{\sigma_{\text{yc}}}{\sigma_{\text{yf}}}\right)^{1/2} - \frac{t}{L}, \tag{8}$$

$$\frac{c}{L} = \frac{1}{2}\left[\left(1+\frac{H}{L}\right)\frac{\tau_{\text{yc}}}{\sigma_{\text{yf}}} - \frac{2t}{L}\right]^{-1}\left(\frac{t}{L}\right)^2 \tag{9}$$

and

$$\frac{c}{L} = \frac{L}{L+H}\frac{\sigma_{\text{yf}}}{\tau_{\text{yc}}}\left[\left(\frac{\sigma_{\text{yc}}}{\sigma_{\text{yf}}}\right)^{1/2}\frac{t}{L} - \frac{3}{2}\left(\frac{t}{L}\right)^2\right], \tag{10}$$

for the transition line between face yield mode and core shear mode, that between face yield mode and indentation mode, and that between core shear mode and indentation mode, respectively. It is clear that these transition lines depend mainly on the strength of face and core materials.

3. Experiments

3.1. Materials and specimens

The core material of sandwich beams is a closed-cell aluminum foam provided by Hong Bo Company, Huaibei, China. Its relative density is 0.17 and the average cell size is approximately 2 mm. The face material is LF21 aluminum alloy (Chinese brand, equivalent to 3003 aluminum alloy in US). The chemical composition of LF21 aluminum alloy and the matrix of aluminum foam are listed in Table 1. The quasi-static engineering stress–strain curves of the foam are shown in Fig. 3. The engineering tensile stress–strain curves

Table 1
Chemical composition of LF21 aluminum alloy and the matrix of aluminum foam (wt%)

	Si	Fe	Mg	Ca	Cu	Zn	Mn
LF21	0.6	0.7	0.05		0.2	0.1	1.0
Aluminum foam	<0.08	<0.12	<0.03	<0.03	<0.005		

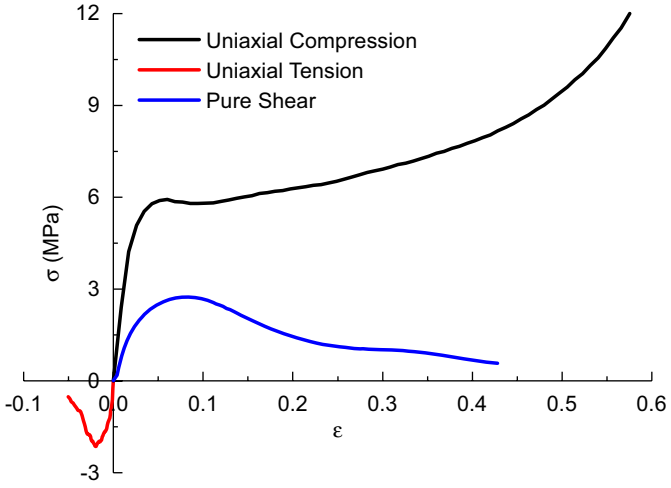

Fig. 3. Engineering stress–strain curves of aluminum foam.

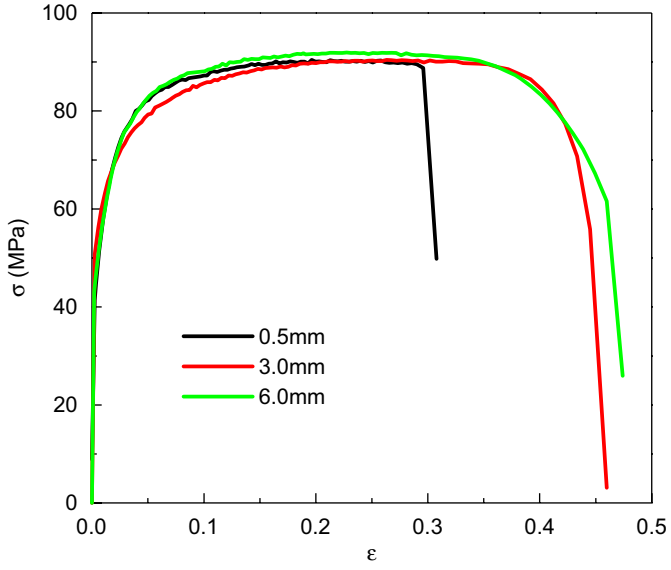

Fig. 4. Engineering tensile stress–strain curves of LF21 aluminum alloy.

Table 2
Mechanical properties of the face sheet and the foam core

(i) Face sheet	
Young's modulus	$E_f = 57\,\text{GPa}$
Yield strength	$\sigma_{fy} = 92\,\text{MPa}$
(ii) Foam core	
Relative density	0.17
Young's modulus	$E_c = 0.65\,\text{GPa}$
Shear modulus	$G_c = 0.12\,\text{GPa}$
Compressive strength	$\sigma_{cy} = 6\,\text{MPa}$
Shear strength	$\tau_{cy} = 2.7\,\text{MPa}$

Table 3
Specimen geometry of three-point bending experiments

Serial number	Total length of beams (mm)	Width of beams (mm)	Face thickness (mm)	Core thickness (mm)	Span (mm)
1	300	30	0.5	10	250
2			0.5	20	
3			0.5	30	
4			0.5	40	
5			0.5	50	
6			3.0	20	
7			3.0	30	
8			3.0	40	
9			6.0	10	
10			6.0	20	
11	300	30	6.0	10	200
12			6.0	20	

of the face material are shown in Fig. 4. The mechanical properties of the face sheet and core are collected in Table 2. The face sheet and foam core are adhered by anti-impact glue SA103.

Different face thickness and core thickness are used. Twelve types of combinations were chosen. The nominal values of specimen geometry are shown in Table 3.

3.2. Quasi-static three-point bending tests

Quasi-static tests were conducted on an MTS810 testing system in the Engineering and Material Testing Center, USTC, using a three-point bending rig at a crosshead speed of 0.1 mm/s. The head of the loading device and the support are all steel cylinders 10 mm in diameter.

Table 4 gives the details of the tests, where P_{max} is the maximum load, and $\tilde{D}_{the}$ and $\tilde{D}_{exp}$ are the theoretical and measured elastic bending stiffness, respectively.

3.3. Low-velocity impact three-point bending tests

Impact tests were conducted on a drop weight machine. The mass of the hammer was 2.58 kg and the drop height was about 1.5 m. This holds an initial impact velocity of about 5 m/s and initial impact energy of about 38 J. The support condition was the same as that in the static tests. The radius of the loading head is 5 mm, identical to that used in quasi-static tests.

An accelerometer was embedded inside the hammer to get the velocity and displacement history. A multi-point average-smoothing method is applied to reduce the 'noise' due to the stress-wave propagation in the hammer. According to a time scale analysis, the upper limiting frequency for the present case is chosen to be 5000 Hz, which will sufficiently reduce the 'noise' but retain the information of bending wave propagation in the sandwich beam. For more details the reader is referred to Ref. [18].

In order to get information of the deformation and failure evolution, a CCD-type high-speed camera SPEEDCAM PRO-LT with a frame rate of 2000 fps was used to record the change of the specimen profile during the test. Rebound and repeated impact of the hammer on the beams were found from the high-speed camera record. However, no further increase in deflection occurred after the first impact. In order to freeze the initial impact failure mode, different 'stop blocks' were used to limit the final deflection when necessary.

Details of the impact tests are given in Table 5, where V_{ini} is the initial impact velocity, δ_p the permanent deflection measured after test and δ_I the maximum displacement of the hammer after the first impact, calculated by integration of the accelerometer signal.

4. Result and discussion

4.1. Failure mechanism

The failure modes observed in the quasi-static experiments are shown in Table 4 and Fig. 5. Three main failure modes studied in Section 2 are distinguished. Debonding between face sheet and core is seldom observed in all experiments. Since the face sheets almost bear all the compressive and tensile stresses in bending, sandwich beams with thin faces are easy to fail in a face yield mode. When the core is thick enough, an indentation mode occurs firstly, but the sandwich beams will finally collapse in a face yield failure mode under sufficient impact energy. If face sheets are too thick and too strong to be crushed, a core shear mode will occur.

The failure mode map according to the strength and geometry data of the face and core materials and the failure modes observed in quasi-static tests are compared in Fig. 6. Two sets of transition lines, associated with different spans used in the tests, are constructed in the graph. Good agreement is observed for all specimens except those with a 3 mm face sheet and 20 mm core. These specimens collapsed in an indentation mode, not the face yield mode as predicted theoretically. One possible reason is that the theoretical analysis does not consider the interaction between the failure modes.

Table 4
Summary of the experimental results of quasi-static tests

Specimen number	c (mm)	t (mm)	b (mm)	P_{max} (KN)	$\tilde{D}_{exp}$ (N/mm)	$\tilde{D}_{the}$ (N/mm)	Failure mode
1062	10.42	0.5	30.48	0.28914	159.35	132.36	FY
1065	9.92	0.5	30.46	0.29276	156.13	121.42	FY
1069	10.20	0.5	31.74	0.32433	167.68	132.80	FY
2046	20.18	0.5	30.77	0.72024	466.24	413.87	FY
2057	20.00	0.5	30.40	0.69073	479.95	402.83	FY
2060	20.12	0.5	30.98	0.63458	516.27	414.63	FY
3013	28.04	0.5	29.64	1.19287	1129.69	683.64	FY, IN
3018	31.70	0.5	29.86	1.06559	771.07	837.58	FY, IN
3020	29.40	0.5	30.94	1.07767	828.77	769.92	FY, IN
4012	40.30	0.5	29.62	1.13171	1152.49	1206.66	IN
4019	41.20	0.5	30.58	1.05893	810.32	1288.41	IN
4033	40.12	0.5	30.14	1.25708	1257.74	1219.48	IN
5006	49.27	0.5	29.57	2.46592	1265.19	1629.08	IN
5010	49.62	0.5	30.30	2.49303	1628.49	1686.83	IN
5018	50.96	0.5	28.96	2.41483	1922.13	1676.72	IN
2011	21.14	3.0	29.92	2.53478	1570.05	1181.28	IN
2018	20.78	3.0	31.10	2.61319	1657.04	1206.83	IN
3042	30.20	3.0	30.26	3.39681	2319.32	1713.34	IN
3043	29.46	3.0	30.86	3.27751	2294.14	1703.92	IN
4015	39.74	3.0	30.56	2.84569	2563.79	2286.18	IN
4016	40.78	3.0	30.32	2.67571	2668.74	2328.50	IN
4034	42.41	3.0	31.09	3.26049	2658.19	2484.55	IN
1043	10.92	6.0	29.90	2.30074	1416.91	1139.50	CS
1044	10.48	6.0	30.58	2.37705	1461.99	1140.97	CS
1050	10.40	6.0	30.48	2.83086	1582.68	1132.83	CS
2027	19.23	6.0	30.20	4.04997	2225.48	1618.50	CS
2031	20.83	6.0	30.31	3.86574	2381.55	1716.10	CS
1027*	10.44	6.0	30.86	3.66887	2039.81	1579.06	CS
1047*	11.27	6.0	31.44	4.05187	2093.59	1665.13	CS
2004*	20.28	6.0	31.40	3.50836	2991.60	2305.94	CS
2039*	20.21	6.0	29.92	3.80641	3208.21	2192.38	CS

Note: (1) The span of all tests is 250 mm except those denoted by "*" for 200 mm; (2) "FY"—face yield mode, "CS"—core shear mode, "IN"—indentation mode.

Table 5
Summary of the experimental results of impact tests

Specimen number	c (mm)	t (mm)	b (mm)	V_{ini} (m/s)	δ_p (mm)	δ_I (mm)	Failure mode
1006	9.88	0.5	31.02	5.096	–	–	FY,
1012	10.26	0.5	30.80	5.098	–	–	FY
1058	9.90	0.5	31.28	5.098	–	–	FY
2047	20.16	0.5	31.10	5.071	–	–	FY
2050	19.95	0.5	31.80	5.075	–	–	FY
2052	20.18	0.5	30.43	5.076	–	–	FY
3011	30.68	0.5	30.68	5.054	–	–	FY, IN
3016	30.18	0.5	29.33	5.054	–	–	FY, IN
3026	29.55	0.5	30.58	5.055	–	–	FY, IN
4020	40.02	0.5	29.56	5.031	27.9	28.5	IN
4032	40.23	0.5	31.58	5.033	–	–	IN
4035	39.95	0.5	30.06	5.033	–	–	IN
5008	50.39	0.5	30.50	5.010	23.5	24.0	IN
5015	49.12	0.5	29.54	5.013	21.0	21.5	IN
5019	50.50	0.5	27.69	5.011	16.1	17.0	IN
2005	20.98	3.0	29.44	5.063	12.8	13.5	CS
2009	21.64	3.0	30.82	5.063	12.2	13.0	CS
2012	20.00	3.0	31.02	5.065	12.5	14.0	CS
3023	30.82	3.0	29.90	5.044	9.8	11.0	IN
3041	29.46	3.0	30.96	5.041	8.0	9.5	IN
3067	29.82	3.0	30.36	5.043	8.0	9.5	IN
4009	40.80	3.0	30.40	5.018	8.5	10.0	IN

Table 5 (*continued*)

Specimen number	c (mm)	t (mm)	b (mm)	V_{ini} (m/s)	δ_p (mm)	δ_I (mm)	Failure mode
4024	40.72	3.0	30.82	5.022	9.0	10.5	IN
4028	41.32	3.0	31.03	5.019	11.0	12.0	IN
1030	10.26	6.0	29.40	5.074	10.5	11.5	CS
1032	10.40	6.0	30.30	5.074	9.5	10.0	CS
2013	20.82	6.0	29.74	5.050	9.0	10.5	CS
2028	20.02	6.0	31.16	5.054	7.0	9.0	CS
1008*	10.14	6.0	30.70	5.075	7.0	8.5	CS
1024*	10.00	6.0	29.50	5.076	8.5	10.0	CS
1035*	11.38	6.0	30.50	5.072	7.0	8.0	CS
2019*	20.06	6.0	29.26	5.052	8.0	9.5	CS
2029*	21.24	6.0	29.28	5.052	7.0	8.5	CS

Note: (1) The span of all tests is 250 mm except those denoted by "*" for 200 mm; (2) "–" denotes that the sandwich beam collapsed fully at initial stage; (3) "FY"—face yield mode, "CS"—core shear mode, "IN"—indentation mode.

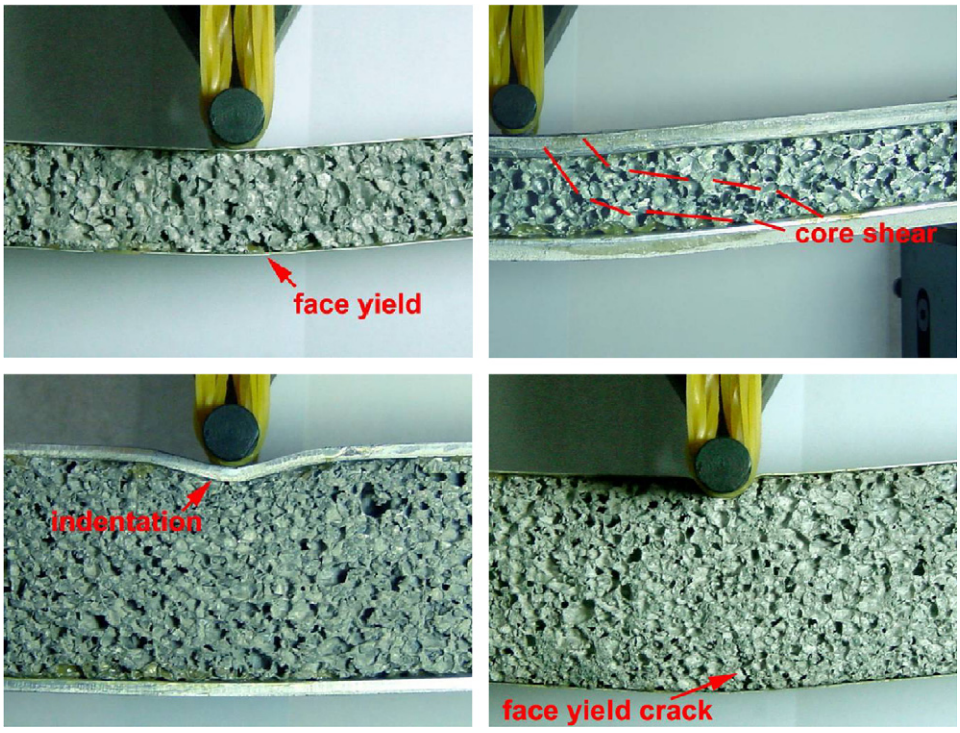

Fig. 5. Failure modes observed in quasi-static tests.

The failure modes observed in the impact bending experiments are shown in Table 5 and Fig. 7. Similar failure modes to those under quasi-static loading are found, but wrinkling of the upper face sheet and debonding between the lower face sheet and the core may occur. However, face wrinkling and debonding appear after the occurrence of the main failure mode when the deflection of sandwich beam is large.

The failure modes observed in the impact tests are also plotted on the quasi-static failure map, as shown in Fig. 8. It transpires that the quasi-static failure map can also predict the failure mode in impact tests. There is also an exception for specimens with a 3 mm face sheet and 20 mm core. These specimens collapsed in a core shear mode. Recall that under quasi-static loading they collapsed in an indentation mode.

Typical force–time curves and corresponding photographs of the impact process of beams failed in face yield, core shear and indentation modes are shown in Figs. 9–11, respectively. These processes are very similar to those under quasi-static loading. However, the force–time curves exhibit large oscillation. Note that the initial peak of the force–time curve is not shown in these figures. It is well known that, due to the inertia effect, a beam under transverse impact will experience larger shear stress than that under quasi-static loading. This explains the face wrinkling and debonding phenomena found in the impact tests. Maybe it is also the reason why beams with a 3 mm face sheet and 20 mm core in the impact tests collapsed in a core shear mode, while those in the quasi-static tests collapsed in an indentation mode.

4.2. Load history

Comparisons of the quasi-static and dynamic force–displacement curves are shown in Fig. 12. The maximum load under the corresponding failure mode predicted by the modified Gibson's model is also shown. Although failure modes are similar between quasi-static and impact bending of the sandwich beams, the force–displacement curves are very different. In all cases, the impact loads exhibit strong oscillation and are higher than the corresponding quasi-static ones, due to the inertial effect, especially the bending wave propagation.

5. Conclusions

Gibson's model is modified to accommodate unsymmetric deformation and cylindrical loading head and supports. Three failure modes, i.e., face yield, core shear and indentation, are assumed. The equations for the corresponding critical loads and a failure map are obtained.

Aluminum alloy skin/aluminum-foam core sandwich beams with different face sheet and core thicknesses are investigated under quasi-static and low-velocity impact loading. Three main failure modes, as assumed in the

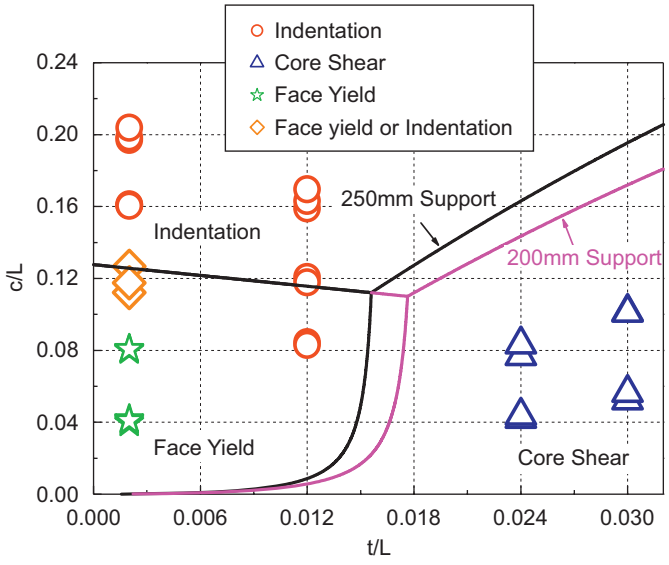

Fig. 6. Comparison of the quasi-static test results and the prediction of modified Gibson's model.

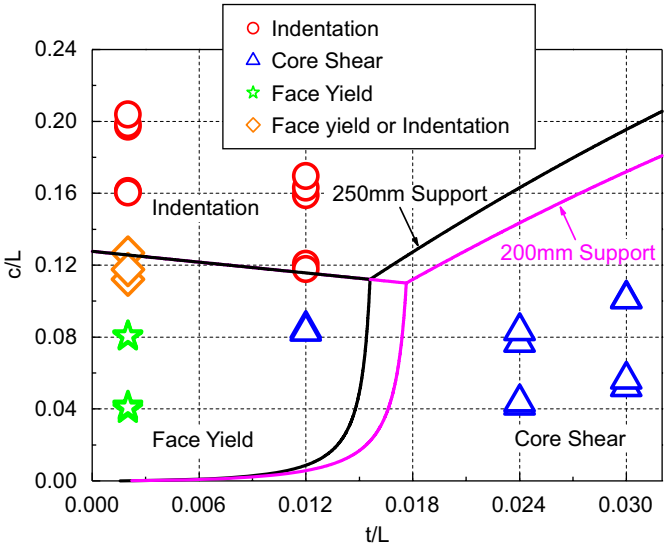

Fig. 8. Comparison of the impact test results with the prediction of modified Gibson's model for quasi-static cases.

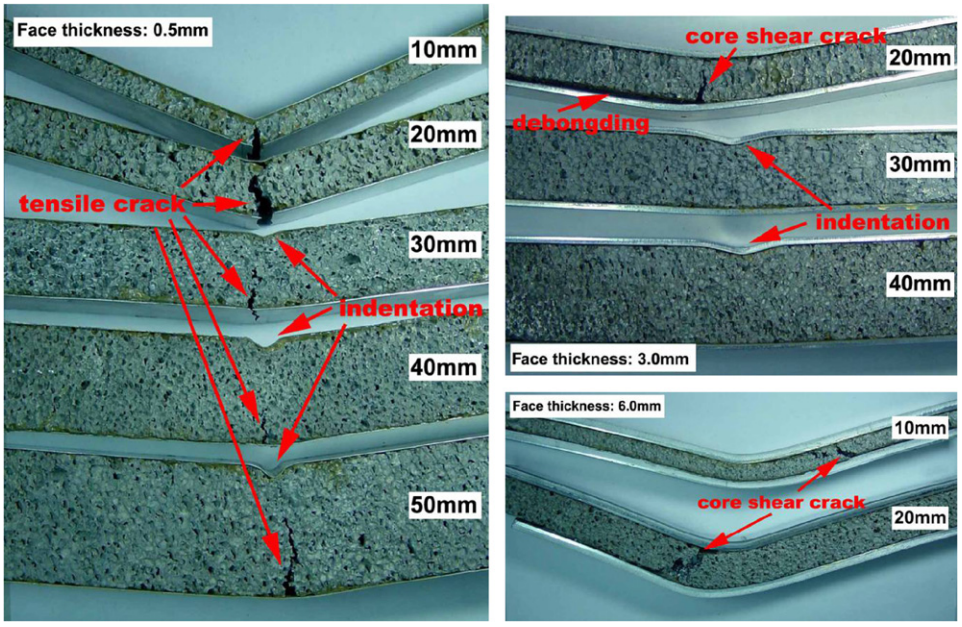

Fig. 7. Failure modes observed in impact tests.

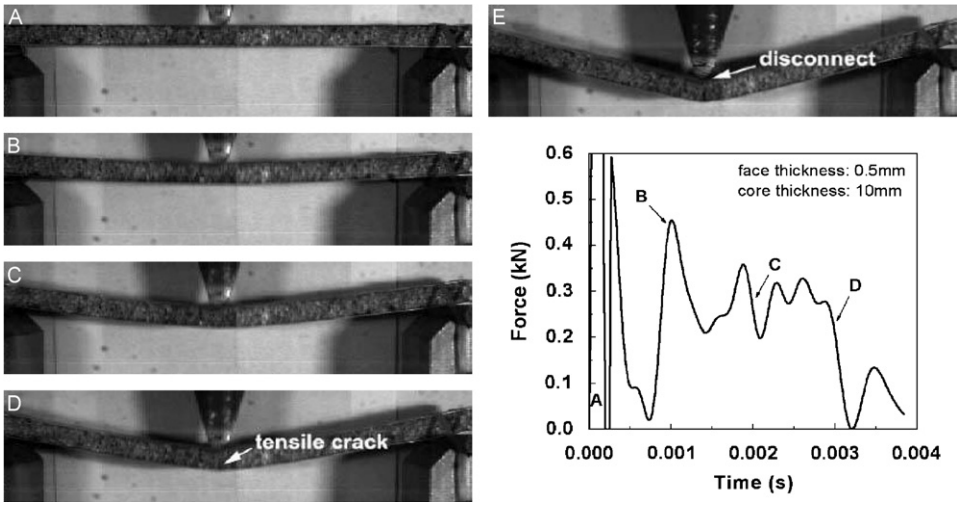

Fig. 9. The force–time curve and photographs of the impact process of a beam failed in face yield mode.

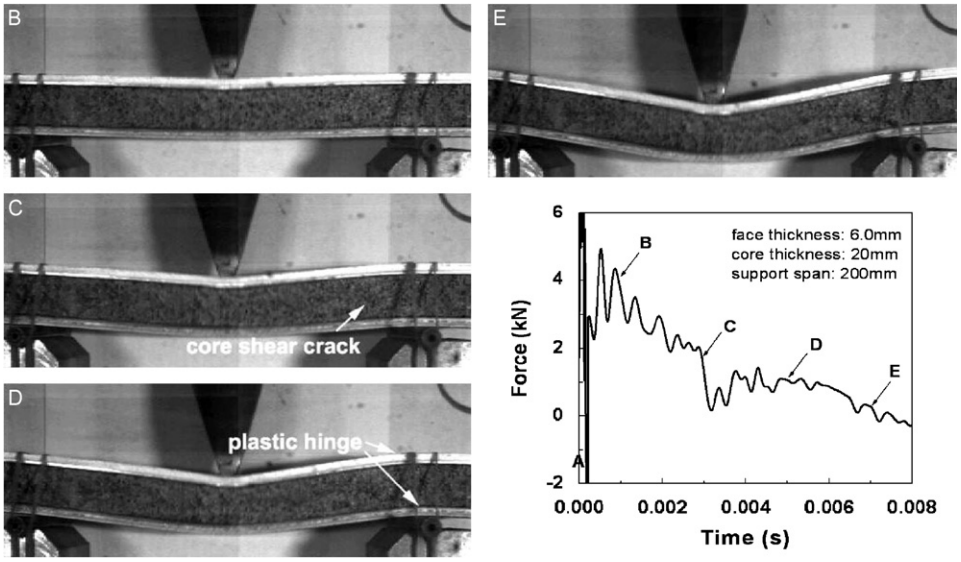

Fig. 10. The force–time curve and photographs of the impact process of a beam failed in core shear mode.

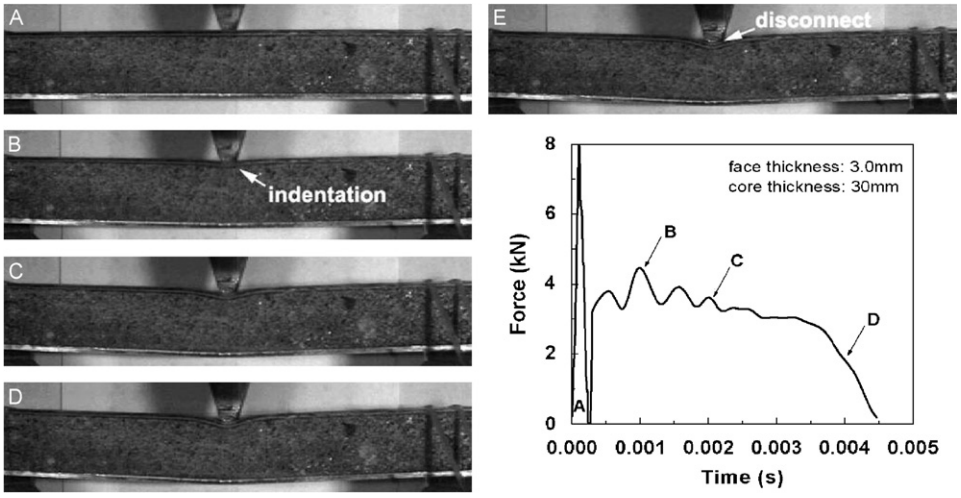

Fig. 11. The force–time curve and photographs of the impact process of a beam failed in indentation mode.

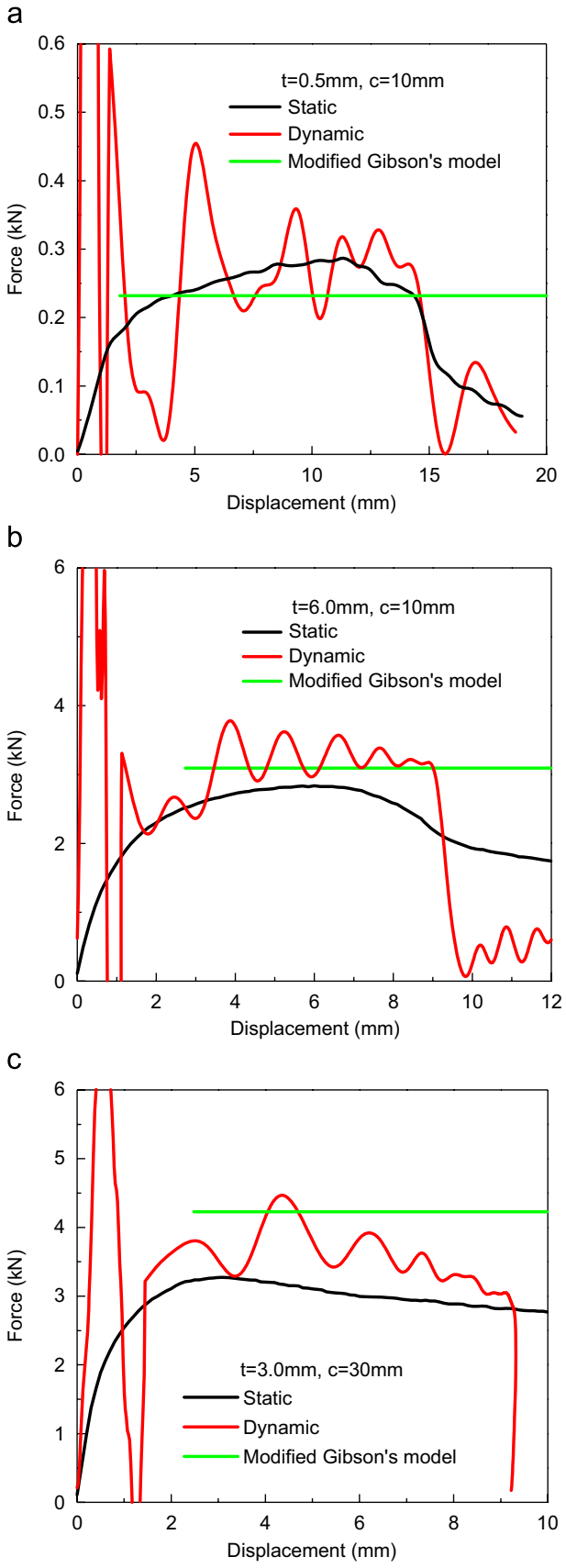

Fig. 12. Comparison of force–displacement curves of foam core sandwich beams under quasi-static and impact loading. (a) Face yield mode, (b) core shear mode, (c) indentation mode.

analytical model, are observed. One exception is beams with thin face sheets and a thick core, which initially failed in indentation mode and collapsed in face yield mode at the end. The theoretical prediction of the failure mode is in good agreement with the experimental results under quasi-static loading. From the high-speed camera record, it is found that the low-velocity impact bending deformation processes and modes are similar to those under quasi-static loading when the impact velocity is lower than 5 m/s. However, the dynamic force–time curves exhibit large oscillation. Nevertheless, the quasi-static failure map can also predict the failure mode of sandwich beams under impact loading. The modified Gibson's model can well describe the maximum load for the face yield mode and core shear mode in quasi-static tests but overestimate the ability of beams failed in an indentation mode. This is because the indentation mode does not consider the degradation of the ultimate resistance to bending of the beam due to cross-section area reduction. Further improvement is required for a better prediction for the indentation mode.

It should also be noticed that the quasi-static model cannot deal with a local and transient effect that occurs under dynamic loading. We did not analyze the dynamic factors such as strain rate effect and inertial effect. These effects may be significant when the impact velocity is high. Also, the range of impact velocities within which the quasi-static model is valid is of interest. It will be a topic for future study.

Acknowledgments

This work is supported by the National Natural Science Foundation of China (Projects 10672156, 10532020, 90205003 and 10302027).

References

[1] Zenkert D. An introduction to sandwich construction. Sheffield, UK: Engineering Materials Advisory Service; 1995.
[2] Abrate S. Impact on composite structures. Cambridge: Cambridge University Press; 1998.
[3] Banhart J. Manufacture, characterisation and application of cellular metals and metal foams. Prog Mater Sci 2001;46(6):559–632.
[4] Degischer HP, Kriszt B. Handbook of cellular metals: production, processing, applications. Weinheim: Wiley-VCH Verlag; 2002.
[5] Gibson LJ, Ashby MF. Cellular solids: structure and properties. Oxford: Pergamon Press; 1997.
[6] Ashby MF, Evans AG, Fleck NA, Gibson LJ, Hutchinson JW, Wadley HNG. Metal foams: a design guide. Boston: Butterworth, Heinemann; 2000.
[7] McCormack T, Miller R, Kesler O, Gibson LJ. Failure of sandwich beams with metallic foam cores. Int J Solids Struct 2001;38(28–29): 4901–20.
[8] Bart-Smith H, Hutchinson J, Evans A. Measurement and analysis of the structural performance of cellular metal sandwich construction. Int J Mech Sci 2001;43(8):1945–63.
[9] Chen C, Harte AM, Fleck NA. The plastic collapse of sandwich beams with a metallic foam core. Int J Mech Sci 2001;43(6):1483–506.
[10] Fatt MSH, Park KS. Dynamic models for low-velocity impact damage of composite sandwich panels, Part B: damage initiation. Compos Struct 2001;52:353–64.

[11] Xu LR, Rosakis AJ. Impact failure characteristics in sandwich structures, Part I: basic failure mode selection. Int J Solids Struct 2002;39:4215–35.
[12] Crupi V, Montanini VR. Aluminium foam sandwiches collapse modes under static and dynamic three-point bending. Int J Impact Eng 2007;34(3):509–21.
[13] Hazizan MA, Cantwell WJ. The low velocity impact response of an aluminium honeycomb sandwich structure. Composites Part B 2003; 34:679–87.
[14] Mines RAW. On the numerical simulation of the progressive collapse of polymer composite sandwich beams under impact loading. Advances in dynamics and impact mechanics. Southampton, Boston: WIT Press; 2003 [Chapter 6].
[15] Besant T, Davies Gao, Huchings D. Finite element modelling of low velocity impact of composite sandwich panels. Composites Part A 2001;32:1189–96.
[16] Lacy TE, Hwang Y. Numerical modeling of impact-damaged sandwich composites subjected to compression-after-impact loading. Compos Struct 2003;61:115–28.
[17] Shipsha A, Hallstrom S, Zenkert D. Failure mechanisms and modelling of impact damage in sandwich beams—a 2D approach: Part II—analysis and modelling. J Sandwich Struct Mater 2003;5(1): 33–51.
[18] Yu JL, Wang X, Wei ZG, Wang EH. Deformation and failure mechanism of dynamically loaded sandwich beams with aluminum-foam core. Int J Impact Eng 2003;28:331–47.
[19] Villanueva GR, Cantwell WJ. Low velocity impact response of novel fiber-reinforced aluminum foam sandwich structures. J Mater Sci Lett 2003;22:412–22.
[20] Xu K, Kou DP, Wang EH, Yu JL. Bending collapse behavior of square aluminum extrusions with aluminum foam filler. Acta Mech Sol Sin 2005;26(3):261–6 [in Chinese].
[21] Villanueva GR, Cantwell WJ. The high velocity impact response of composite and FML-reinforced sandwich structures. Compos Sci Technol 2004;64:35–54.
[22] Qiu X, Deshpande VS, Fleck NA. Finite element analysis of the dynamic response of clamped sandwich beams subject to shock loading. Eur J Mech A/Solids 2003;22:801–14.